UNIVERSITY OF LEEDS

White Rose
university consortium
Universities of Leeds, Sheffield & York

eprints@whiterose.ac.uk
https://eprints.whiterose.ac.uk/

Fabrication of cartilage-inspired hydrogel/entangled polymer-elastomer structures possessing poroelastic properties

Siavash Soltanahmadi[a], Nicholas Raske[b], Gregory N de Boer[a], Anne Neville[a], Robert W Hewson[b], Michael G Bryant[a*]

*M.G.Bryant@leeds.ac.uk

[a] School of Mechanical Engineering, University of Leeds, Leeds, LS2 9JT, UK

[b] Department of Aeronautics, Imperial College London, London, SW7 2AZ, UK

Abstract

The ability to replicate the load bearing properties of articular cartilage is attractive for many engineering applications; particularly bearings where low-friction, low-wear and high durability is required. Hydrogels are widely used materials spanning many diverse applications owing to their lubricity and unique mechanical/chemical properties. The poor mechanical characteristics of conventional hydrogels, especially their compressive behaviour, limit their application in load-bearing applications despite their favourable properties such as poro/visco-elasticity and lubricity. This paper demonstrates a cartilage-inspired approach to produce a structure which benefits from water-swelling resistant and ultrafast recovery behaviour of elastomers as well as the stress-relaxation and energy dissipation properties of hydrogels. A method is presented in this work to fabricate interconnected macro-porous elastomers based on sintering polymethylmethacrylate beads. The porous elastomer imparted structural support and resilience to its composite with infused-grafted hydrogel. At 30% strain and depending upon the strain rate, the composite exhibited a load-bearing behaviour that was 14 to 19 times greater than pristine hydrogel, and approximately 3 times greater than the porous elastomer.

The equilibrium elastic modulus of the composite was 452 kPa at a strain range of 10%-30% which was close to the values reported for the modulus of cartilage tested with similar experimental parameters defined in this study. The dissipated energy for the composite at strain rates of 1 s^{-1}, 10^{-3} s^{-1} was enhanced by 25, 25 and 5, 15-fold as compared to that for the pristine hydrogel and the porous elastomer, respectively. The cyclic loading tests at two strain rates showed that the composite immediately recovers its load-bearing properties with the maximum load recovery staying above 95% of its initial values throughout the testing. The permeability of the structures were measured experimentally and results showed a decrease of permeability by three orders of magnitude following hydrogel grafting.

Keywords
Poroelastic; Bio-inspired hydrogel; Cartilage rehydration; Stress relaxation; Tough hydrogel composite; Polyacrylamide gel; Polydimethylsiloxane sponge

Introduction
Articular cartilage is an impressive natural material that can withstand high contact pressures relative to its modulus with minimal friction and wear[1]. Acellular cartilage is a bi-phasic system[2] composed of crosslinked collagen fibres with embedded coiled proteoglycan chains[3]. The solid matrix of acellular

cartilage retains the second phase, i.e. synovial fluid and thereby dissipates energy upon loading. One of the unique characteristics of cartilage which distinguishes it from engineering systems is its load-bearing behaviour. Cartilage can bear contact pressures greater than its compressive modulus[1]; facilitated through fluid pressurisation within its porous structure[2]. It is hypothesised that the lubricity of cartilage is mainly attributed to surface-tethered macromolecules at lower sliding speeds[4] and fluid pressurisation at higher sliding speeds[1]. As a result, there has been a vast amount of research focused on mimicking its superficial characteristics through grafting hydrophilic brush-like polymer chains (i.e. grafted polymer chains) including zwitterionic[4-5] and polyacrylamide (PAAm) grafted polymer chains[6] or hydrogels[7]. This includes studies which focused on the integration of hydrogels on the lubricating surface (up to few microns in thickness) of the material[8]. Surface grafted polymer chains/hydrogels have been shown to impart lubricity through a hydration/water-film mediated lubrication mechanism[9]. Further, a substantial number of studies have focused on mimicking cartilage lubricity via surface tethering of polymeric chains to harder substrates [4-5, 8, 10]. However, these surface engineering strategies do not completely address the load-bearing properties of cartilage inspired systems and concerns about their durability have been raised. Translation of this load bearing behaviour to real engineering materials has attracted a considerable body of research through design and formulation of reinforced hydrogels[3, 7, 11-18].

Unmodified hydrogels generally possess poor compressive strength[17] and cannot withstand the high loads often encountered in engineering and biomedical load bearing applications[8]. Highly stretchable and mechanically tough hydrogels have been created through strategies such as polyrotaxane gels[19], nanocomposite gels doped with water-swellable inorganic clay[20], double-network (DN) gels[21] with low friction characteristics[15], macromolecular microsphere gels[22], tetra-poly(ethylene glycol) gels[23] and supramolecular hydrogels[24]. Supramolecular hydrogels composed of polyampholytes with ionic bonds of weak and strong strength provide Young's modulus on the order of MPa and have been boosted with self-healing characteristics[24]. Initial DN gels, macromolecular microsphere gels and tetra-poly(ethylene glycol) gels, have not achieved a comparable elastic modulus to cartilage. DN gels exhibited high elastic modulus at strains above 50% where cartilage shows macroscopic tears[21]. Macromolecular microsphere gels benefited from structural integrity at strains up to 99.7%, however showed a low compressive stress of 60 kPa at 50% strain[22]. A high strength at maximum breaking point (9.6 MPa) was reported for tetra-poly(ethylene glycol) gels, while having a mediocre compressive modulus of 40 kPa[23]. In follow-on works, DN gels with enhanced strength have been prepared by ionic crosslinking of alginate/chitosan in polyacrylamide matrix[25-27], the mechanical properties of which exceed those of previous DN gels.

Conventional DN hydrogels have rarely brought a significant improvement to the mechanical properties in an equilibrium state (i.e. fully-swollen). They often require further improvements such as the incorporation of crosslinks through metallic coordination complexes which yielded a tensile modulus of around 2 MPa[28]. Subsequently, remarkable increases in tensile[29-31] and compressive[7] strengths were bestowed on hydrogels via metal ionic dual cross-linkage. In addition, enhanced mechanical properties have been prompted by hydrogen bonding between functional groups of polymer chains. Clustering of polymer aggregates via hydrogen bonding between copolymer chains of N,N -dimethylacrylamide and meth-acrylic acid have been shown to generate highly rigid and tough hydrogels with a tensile modulus of 28 MPa and recovery time of approximately one hour[32]. Recent work by Wang et al [33] showed that the tensile elastic modulus and pH range can both be extended up to few hundreds of MPa and alkaline values of <9.6. The calcium phosphate mineralisation of hydrogels[34] is another developed strategy to achieve hybrid hydrogels with compressive modulus of few hundred MPa.

A modified double-layer hydrogel, with friction and load-bearing characteristics similar to cartilage, was synthesised by Lin et al.[7] This was achieved through a stiff hydrogel substrate obtained by the formation of ionic coordinates between ferric ions and the carboxyl groups from poly acrylic acid. The resulting structures had extremely high compressive strength and exhibited a compressive modulus of over 6 MPa[7]. The Young's modulus was approximately an order of magnitude larger than cartilage[35-37] and self-recovery of the hydrogels occurred within few hours at room temperature[30] which is a weak point for the hydrogel. Hydrogels improved by metal-ligand coordination have been recently advanced by Xu et al. [38] through dual covalent and physical crosslinking of a poly(2-isopropenyl-2-oxazoline) hydrogel with up to an 11-fold increase in compression modulus through Zn^{+2} complexation. This hydrogel had a faster recovery process that could recover 98.5% of its initial size and mechanical response following re-swelling in deionized water for 60 minutes. Another group of hydrogels developed to deliver compressive properties close to that of cartilage are interpenetrating network hydrogels (IPN)[11, 13]. 3D woven IPN composites of agarose infused polyglycolic acid[11] and alginate/polyacrylamide infused poly(ϵ-caprolactone)[13] have been generated compressive and shear moduli on the order of native cartilage (Young's modulus in unconfined compression tests was between 68-77 kPa and 200 kPa for the former and later respectively). This was used for cartilage tissue engineering and these two materials exhibited moduli within the lower threshold of that of articular cartilage.

Cartilage is a complex bi-phasic structure with load-bearing properties and stress-relaxation characteristics considerably closely related to its water content[39]. The stress-relaxation response of cartilage is indicative of the load carried by the pressurised fluid within its structure and hence its unique load-bearing behaviour[2]. The low-friction characteristics of cartilage are rooted in its poroelasticity[1-2] and water-retaining macromolecules within the structure[4]. The porous structure of cartilage facilities its re-hydration promoting fluid pressurisation[1-2]. Studies have shown that the mechanical properties (including stress-relaxation characteristics) can be correlated to osteoarthritis[40]. Therefore, the poro-viscoelastic stress-relaxation response of a structure aiming to mimic cartilage is of paramount importance. Embedded/grafted hydrogels/brushes[41] on stiff substrates lack the poro-viscoelastic relaxation observed in natural cartilage which is an essential factor for lubrication[1]. On the other hand, hydrogel-based systems can represent the poro-viscoelastic relaxations. While there have been numerous successful efforts to improve the mechanical properties of hydrogels, examining the stress-relaxation behaviour of hydrogels has not been wide-reaching[42-43]. Visser et al.[42] fabricated a gelatine methacrylamide hydrogel infused into electrospun poly(ϵ-caprolactone) scaffolds and showed that the time-dependant stress-relaxation and mechanical parameters of the composite were similar to cartilage in unconfined compression. The equilibrium modulus (i.e. modulus calculated from the data for equilibrium stress and strain curve after full stress-relaxation processes) of this hydrogel infused scaffold tends to approach that of the hydrogel alone and was smaller than that of cartilage following fast loading. However, the stress-relaxation time scale was very similar to cartilage. Another study by Sun et al.[43], investigated the stress-relaxation of a modified hydrogel comprising of PAAm and supramolecular peptides which showed two distinct relaxation time scales comparable to cartilage[43]. The equilibrium stresses (i.e. stress at a defined strain after a full stress-relaxation process) were reported to reach values between 70%-90% of the peak stress[43] (the maximum stress at a defined strain limit) which showed inferior stress-relaxation capacity when compared to cartilage where the maximum load was relaxed by up to 90%[2].

It is clear that more research is required to create multi-phase structures that can embrace the disparate package of properties found in cartilage (e.g. stress-relaxation and tribological behaviour, high modulus and stress-recovery). This is vital to achieve translation of articular cartilage lubrication and load-bearing theories towards functional engineering systems. This work aims to integrate the

structural characteristics of cartilage with its pressure-driven poroelastic behaviour to produce functional bio-inspired load-bearing structures. The materials framework described herein paves the way for a new generation of soft-matter, multi-phase, multi-material systems with enhanced and tuneable loading bearing properties. A stratified approach to produce a porous multi-phase material with enhanced load bearing capabilities was adopted. In this view, the developed material systems shares structural similarities with cartilage; a crosslinked network of collagen microfibers with a second network of coiled proteoglycan chains that could dissipate energy through poro-viscoelasticity[3] with the possibility to further tuned to infer superior lubrication properties. In contrast to the aforementioned research, this work focusses on the integration of existing polymer chemistries and our knowledge of poroelastic behaviour of cartilage to engineer and demonstrate a bi-phasic, cartilage-inspired material system for engineering applications (i.e. journal bearings).

Osmotic pressure-driven swelling often leads to weakening of hybrid hydrogels[16] causing mechanical instability. Shape recovery has been the other challenge with modified hydrogels beside the loss of mechanical properties once swollen. The fastest recoveries take minutes to occur and do not result in a return to the hydrogels' initial properties[44]. In this paper, we demonstrate that a hydrophobic crosslinked elastic matrix fabricated from polydimethylsiloxane imparted immediate recovery to the composite after unloading. This occurs with no need for re-swelling time which is an advantage compared to previous hybrid hydrogel systems[3]. Further, the infused hydrogel was confined by the stiffer structure of the elastomer which restricted swelling and hence mitigated the loss of mechanical properties. The composite was stiffer than either the porous elastomer or hydrogel alone with an equilibrium compressive modulus (0.452 MPa at 10%-30% strain) in the range of the modulus values reported for human cartilage (equilibrium unconfined modulus of 0.3-0.9 MPa at 15%-25% strain). The inclusion and mechanical/chemical retention of the hydrogel is expected to promote enhanced and durable lubrication.

Materials and methods

Materials

Polydimethylsiloxane (PDMS) sponges were prepared using Silicone Sylgard 184 Kit (Dow-Corning, USA) and un-crosslinked polymethylmethacrylate (PMMA) spherical powder purchased from Goodfellow. The PMMA had a mean particle size of 48 μm and used following an air jet classification process by Hosokawa Micron (see Figure S 1 in the supporting information; SI). The PDMS monomer solution and its curing agent were mixed at a weight ratio of 10:1 as recommended by the supplier. Acrylamide (AAm, 99+% ; Alfa Aesar), N,N'-methylenebisacrylamide (MBAA, 99+%; Alfa Aesar) as a crosslinker and 2-hydroxy-4'-(2-hydroxyethoxy)-2-methylpropiophenone (Irgacure 2959, 98%; Sigma-Aldrich) as a photo-initiator were used as-received to fabricate the end-grafted PAAm (EGP)/gel-PDMS materials. 3-(trimethoxysilyl)propyl methacrylate (TMPM, 98%; Sigma-Aldrich), hydrochloric acid (37% solution in H_2O; ACROS Organics), ethanol (absolute, 99%+, Fisher Chemical), hydrogen peroxide (30% solution in H_2O; Sigma-Aldrich) were purchased from indicated suppliers for silanisation process.

Fabrication of PDMS sponge

Cylindrical stainless-steel moulds which were 16 mm in length and had a bore diameter of 6.35 mm were used to fabricate the PDMS sponges. The PDMS was infused to create the composite of PDMS and PMMA particles and then milled to a 10mm length, separating it from the circular bases. This resulted in open porosity on the two circular faces and an impermeable cylindrical surface along the length. PMMA particles were heat sintered at 180°C for 90 minutes and PDMS was incubated in an air-circulated oven at 100°C for 30 minutes for the curing process.

PAAm grafting into the PDMS sponge

The PDMS sponge was washed in acetone using an ultrasound bath for 15 mins and dried overnight under vacuum. The washed PDMS sponge was etched in a solution of HCl(37%):H_2O_2(30% w/w):H_2O (volume ratio 1:1:1) for 1 hour at room temperature in order to create silanol groups on PDMS surfaces. The etched PDMS sponge was then rinsed with plenty of de-ionised (DI) water several times and dried under nitrogen gas flow. The TMPM silanisation of the PDMS sponge was conducted using a solution of C_2H_5OH:TMPM:H_2O (volume ratio 2:1:2) for a total duration of 330 minutes comprising three steps of 1) 120 minutes ultra-sonication at 40-45˚C, 2) 180-minute standstill at room temperature and 3) 30 minutes of annealing process at 70˚C under ultra-sonication. The silanised PMDS sponge was rinsed in plenty of DI water, isopropanol and ethanol several times with a final step of ultra-sonication in ethanol for 5 minutes to remove the excessive un-bonded or physically adsorbed TMPM. The silanised sponge was vacuum dried overnight prior to PAAm grafting.

For PAAm grafting 3M of AAm (2.13 gram) was dissolved in 10 mL of pure water in a nitrogen-gas filled glove-box. The pure water was nitrogen bubbled for more than 30 minutes prior to addition of AAm. The PDMS sponge was infused with the AAm solution and UV treated for 2 minutes before adding 3.75 mM (8.4 mg) of 2-Hydroxy-4'-(2-hydroxyethoxy)-2-methylpropiophenone photo-initiator. UV irradiation was performed for 90 minutes in the solution of AAm and the photo-initiator to achieve the EGP-PDMS composite. The gel-PDMS composite was obtained through 60 minutes of UV exposure in a solution of AAm, MBAA crosslinker and the photo-initiator with a molar concentration of 3M, 0.5 mM and 3.75 mM respectively.

UV treatment

The polymer chain/gel grafting was conducted at room temperature using a UV lamp (UVP, XX-15L, 15 W,) incorporated with a 365 nm wavelength filter (UVP, XX-15L) at a 5 cm distance delivering an irradiation intensity of 7.27 mW/cm². The PDMS sponge was partially transparent to the UV wavelength range irradiated by the lamp (see Figure S 2 in the SI). UV treatment was carried out in a sealed glove-box purged with N_2. In order to minimise oxidative reactions, pure water was nitrogen bubbled for at least 30 minutes before the monomer and photo-initiator were added. Following the polymer chain/gel grafting, samples were placed in pure water-filled plastic vials (50 mL) for 96 hours to remove any traces of the unreacted/ungrafted monomer, crosslinker, photo-initiator molecules and impurities. The pure water was replaced every 24 hours.

ATR-FTIR analysis

A Spotlight 400 (Perkin-Elmer, USA) Attenuated Total Reflection - Fourier Transform Infrared (ATR-FTIR) spectrometer was used to ascertain complete removal of the PMMA particles for PDMS sponge fabrication and to confirm PAAm grafting onto the pore surfaces inside of the PDMS sponge. ATR-FTIR scans were obtained over wavelengths of 700 cm^{-1} to 4000 cm^{-1}. The peak positions were identified using the Peak Analyser tool in Origin (OriginLab Corporation) following a Savitzky-Golay smoothening function of polynomial order 2. The identified peaks were cross compared with the spectra from reference materials and the reference spectra taken from the Sigma library of FTIR. Materials were dehydrated in an oven at 45˚C for 48 hours in order to rule out significant contribution of OH groups from water. Samples were gently compressed onto the detector crystal to obtain signals from several micrometres into the structure [9].

Tensiometry

A computer controlled and programmable video-based contact angle and surface tension meter (CAM 200, KSV Instruments) was used to track and record dynamic water contact angle measurements. Images were captured over an interval of 20 minutes to assess the water intake and wettability behaviours. WCAs were obtained immediately after a 20 µL water droplet had landed on the fully-hydrated material surfaces (except the PDMS sponge) and every minute after the droplet exposure. WCA was acquired for a minimum of three spots on surfaces for each sample and the average of the measurements was reported. The WCA measurements were carried out on the end faces of the sample. The materials had been submerged in pure water prior to the measurement.

Electron microscopy

Scanning electron microscopy (SEM) and Cryo-SEM was undertaken using a Carl Zeiss EVO MA15 and a Thremofisher Helios G4 CX DualBeam monochromated field emission gun instruments respectively. A 10-nm layer of iridium was deposited on the PDMS sponge samples before SEM imaging at an acceleration voltage of 20kV. For cryo-SEM a block of samples (ø: 5mm, L: 5 mm) was cut from the middle of the bulk and placed into a cryo-SEM shuttle surrounded by an adhesive of optimum temperature cutting medium and colloidal graphite. The sample was plunged into slushed nitrogen (solidified at around -210˚C under vacuum) using a Quorum Technologies PP3010 cryo-SEM preparation system. The samples were allowed to cool to the liquid nitrogen temperature. Samples then were immediately transferred to the preparation chamber which was pre-cooled to -140˚C at a pressure of 5×10^{-7} mBar. The samples were fractured using a cooled knife and sputter coated with iridium. The cryo-fractured and coated samples were then transferred to the main chamber of the cryo-SEM operating at -140˚C. The samples were imaged at an acceleration voltage of 2kV and a beam current of 0.1nA. The EGP-PDMS sample was subjected to one step of sublimation at -90˚C for 3min to reveal the PAAm chains.

Permeability measurements

A cell was designed and developed in-house to measure permeability of the materials. The cell was embedded in a setup comprising a syringe pump (Cole-Parmer 74900), integrated with a glass syringe (Eterna Matic Sanitex, EM304), and a manometer (Digitron P200M) connected to the cell through nylon tubing and pneumatic fittings (see Figure S 3 in the SI). The developed materials (ø:5mm, L: 5 mm) were mounted in the cell and the pure water was injected into the cell at a defined flow rate. The pressure drop between the inlet and outlet, resulted from the fluid flow through the material, was monitored and recorded for 5 mL of water injection (logging every 10 s) and eventually averaged. The pressure drop for each material was determined at three flow rates. The flow rates for the PDMS sponge were 0.1, 0.4 and 0.6 mL/min, for the EGP-PDMS were 0.01, 0.04 and 0.06 mL/min and for the gel-PDMS were 0.001, 0.004 and 0.006 mL/min so that the pressure drop readings remained within a relatively similar range for all materials. A continued flow of water was maintained until the reading stabilised (fluctuation <±5% of the reading value) and then recorded for calculation of the permeability. The permeability of the materials were solved using Darcy's law of permeability (Eq. 1)

$$Q = \frac{\kappa}{\nu} \nabla p \quad (1)$$

Where Q is the fluid flux (flow rate per unit area; m/s), κ is permeability (m^2), ν is the fluid viscosity (Pa.s), p is the fluid pressure (Pa) and ∇ is the gradient operator. The permeability for each material (3 samples for each material) was determined by a linear regression of the plotted graph of the differential pressure data against the flow rate data.

Compression tests

Load-bearing properties of materials were assessed using a Universal Mechanical Tester (UMT, Bruker) equipped with a DFH-5-G (2.5 mN resolution) force sensor and a Mecmesin MultiTest mechanical tester hosting a load cell with a maximum capacity of 1kN (resolution: ±0.2%). The testing procedure consisted of four phases, namely tare loading, fixed-distance loading, hold (pause) and unloading phase. The tare loading was conducted at a relatively low strain rate of 10^{-3} s^{-1} to maintain equilibrium. Tare loads (pre-load prior to the actual loading phase) of 0.2N and 0.5N were used for tests using UMT and Mecmesin instruments respectively. Within the loading phase samples were compressed to a certain strain limit (10%-50%) at 10^{-3} s^{-1}, 1 s^{-1} and 16x10^{-3} s^{-1}, 0.83 s^{-1} for tests using UMT and Mecmesin respectively. The materials then remained compressed at the defined strain for 12 hr and 15 s in UMT and Mecmesin tests respectively allowing stress-relaxation to occur. The applied strain was released within the unloading phase. The same strain rate was used for loading and unloading phases in each compression test. In order to examine load-recovery properties of the materials, cyclic loading experiments were carried out using the Mecmesin with a pause phase of 15 s. Following on from the 1st loading cycle, the next consecutive cycles instigated immediately either from the defined tare load (section 'Cyclic compression testing behaviour of the materials') or from the absolute zero condition (the flat plunger was fully retracted to a zero load condition; shown in Figure S 4 in the SI).

The set-up developed for compression testing comprised a flat porous indenter, a flat porous drainage plate (placed at the bottom side of materials) and a cylindrical water bath (see Figure S 5(a and b) in the SI for more information). The materials (i.e. PDMS sponge and EGP/gel-PDMS) were impermeable on the cylindrical surfaces along the length (Figure S 5(c)) and hence were confined in terms of fluid flow which was only allowed in and out the cylindrical bases but mechanically unconfined to allow deformation. The materials were soaked in pure water at least 48 hr before tests. The samples (except dry-PDMS) were fully immersed in a water bath during compression tests. The pure water was forced into the pores within the PDMS sponge samples under vacuum, while the samples were placed in a water-filled beaker.

The following two-term exponential decay function was used to fit the load-log(t) graphs at 30% iso-strain to obtain time constants[45] (Eq. 2).

$$y = y_0 + \mathrm{A}e^{-t/\tau_1} + Be^{-C(t/\tau_2)^D} \quad (2)$$

Where y_0 is the load value (N) after the full stress-relaxation, t indicates time in the pause phase (s), A and B are coefficients correlated to y_0 (N), C and D are coefficients associated with geometric compression and the strain limit and τ_1 and τ_2 represent characteristic short-term and long-term stress-relaxation time scales respectively. The 6 fitting parameters include A, B, C, D, τ_1 and τ_2. The built-in non-linear curve fitting tool in Origin (OriginLab Corporation) was used for stress-relaxation curve fitting. Time was set to zero at the maximum stress value once the strain reached the 30% limit. The goodness of fit for the least squares fitting algorithm was evaluated by residual plots, residual sum of square and adjusted R-square values. The sum of the squared error between the actual data points and the best-fit curve were compared to global minima.

The elastic compressive moduli were calculated by linear regression of the resultant stress-strain curves for peak-load (i.e. the maximum load recorded at a defined strain limit) and when equilibrium (i.e. the load recorded after complete stress-relaxation processes at a defined strain limit) was reached. The strain rate for these experiments was 0.83 s^{-1}. The compressive moduli were obtained

within two strain brackets where a linear stress-strain response was observed (i.e. 0.1-0.3 and 0.3-0.5). The Pearson's r value for the statistical analyses was always greater than 0.98.

The area under the loading and unloading curves and between the tare strain and 30% strain were obtained by calculation of definite integrals. The difference between the area under loading and unloading curves following the 12 hr hold phase is the full-capacity energy dissipation. These tests were conducted with the UMT tester and at two strain rates of 1 and 10^{-3} s^{-1}. For ease of comparison, full-capacity energy dissipation value for each material was divided by the value for PAAm gel (i.e. normalised to PAAm gel). The normalised values are outlined in the result section (section 'Compressive modulus of the materials') denoted as "dissipation enhancement ratio". Also, the ratio of the energy dissipation at the low strain rate (10^{-3} s^{-1}) to that at the high strain rate (1 s^{-1}) was obtained for each individual material and presented as "dissipated energy ratio". For cyclic compression tests, which were carried out using the Mecmesin instrument at strain rates of 0.83 and 16×10^{-3} s^{-1}, a 15-s hold phase was considered. This indicates that the dissipated energy values for the PDMS sponge represent its full-capacity energy dissipation, however for the gel-PDMS material the values reflect dissipated energy after the first (short time-scale) stress-relaxation.

Results and discussion

Preparation of the porous elastomer

A new facile method based on the template leaching technique was developed in this study for producing poroelastic PDMS materials. In this three-step process, PMMA spherical particles were casted into glass-slide bottomed cylindrical stainless-steel moulds and transferred to an air-ventilated oven. The PMMA particles were heat-sintered at a temperature above its glass transition to produce a template for the porous elastomer. The heat sintering induced necking of the PMMA beads through viscous flow of particles into the neighbouring particles. This produced a network of particles which were 3-dimensionally fused into their surrounding particles. A degassed solution of PDMS elastomer and its curing agent was then used to backfill gaps between particles in a vacuum chamber followed by heat curing of PDMS in an oven. The cylindrical composite of perfused PDMS and PMMA particles was then immersed into an organic solvent (i.e, acetone, ethyl acetate and/or dimethylformamide) and sonicated in a bath for few hours to reveal a porous PDMS (so-called PDMS sponge). The pores formed a network that was interconnected at the sites where the PMMA beads were fused. The complete dissolution and removal of the PMMA (i.e. the template) was examined by ATR-FTIR as shown in Figure S 6 of the SI. Dissolution of PMMA particles generated an interconnected porous matrix of PDMS elastomer. A summary of the process and an electron micrograph of the fabricated PDMS sponge are shown in Figure 1. Energy dispersive X-ray spectroscopy was conducted on the PDMS sponge to demonstrate spherical porosity of the sponge through chemical mappings (Figure S 7 in the SI).

The procedure is sustainable as the PMMA can be retrieved by solvent extraction (Figure S 8(a and b) in the SI). The pore sizes can be tuned with the PMMA particle size. The pore size, interconnectivity and interfacial properties impact the mechano-chemical properties of the porous PDMS[46]. To attain a facile method for producing poroviscoelastic structures, as-prepared PMMA powder with an average size of 48 um was randomly packed in the mould. Otherwise, ordered 3D structures of a PDMS sponge could be produced by colloidal crystal templating[46-49]. This could be achieved through forming close-packed arrangements of particles using colloidal suspensions of monodispersed PMMA particles [48]. For example, macroporous poly(ethylene oxide) dimethacrylate hydrogel in a 3D ordered arrangement has been prepared from PMMA colloidal spheres [47].
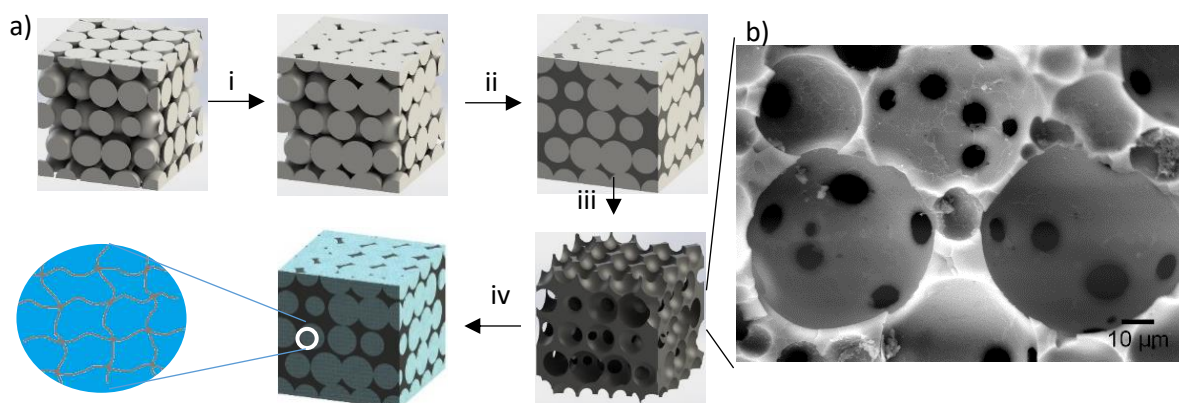
Figure 1. a) Schematic of the fabrication method for the PDMS sponge. The numbered arrows are associated with: i) sintering of the PMMA particles, ii) PDMS backfilling, iii) dissolution of PMMA particles out the structure and iv) side polymer chain/hydrogel graft-infusing into the PDMS sponge. b) An electron image of the PDMS sponge.

EGP/hydrogel functionalisation of the poro-elastic elastomer

TMPM silane groups were used to graft PAAm side chains/hydrogel onto the hydrophobic pore surfaces of the PDMS sponge. The procedure for chemical grafting and cryo-SEM images of the silane/EGP/hydrogel-grafted PDMS sponge are shown in Figure 2. The reaction paths to etch, silanise, brush and gel graft PDMS sponges are elucidated in sub-panels i, ii, iii and iv of Figure 2(a) respectively. The PDMS sponge was etched in order to create silanol groups on the PDMS surfaces facilitating silanisation (the sub-panel i in Figure 2(a)). The hydrolysis and condensation of TMPM led to silanisation of the PDMS sponge[50]. The silanisation created grafting of individual TMPM and crosslinked TMPM groups onto the etched PDMS surfaces (the sub-panel ii in Figure 2(a)).

Chemical grafting of PAAm side chains/hydrogel to the PDMS sponge was carried out via free-radical polymerisation of AAm monomers using a photo-initiator. Illustrated within the sub-panel iii in Figure 2(a), the PDMS sponge was placed in a solution containing AAm and the photo-initiator and then irradiated with UV light to create the EGP-PDMS composite. The gel-PDMS composite was obtained through UV irradiation in a solution of AAm, MBAA crosslinker and the photo-initiator, the sub-panel iv in Figure 2(a). A 20-90 nm thick interfacial layer was observed in cryo-SEM images as marked in Figure 2(b) (in between two yellow-coloured dashed-lines). This distinct layer was also found in cryo-SEM images for EGP/gel-PDMS sponges (Figure 2(c and d)) and can be attributed to the etched-silanised surface. A cryo-image from a pristine PDMS sponge is provided in SI (Figure S 9) evidencing the absence of the silanised interfacial layer. Grafted polymer chains and crosslinked PAAm chains are visible in Figure 2(c and d) where they extend out from the PDMS interface towards the internal area of pores. The silanised layer and PAAm grafting were confirmed by the ATR-FTIR results (Figure 3(a)).
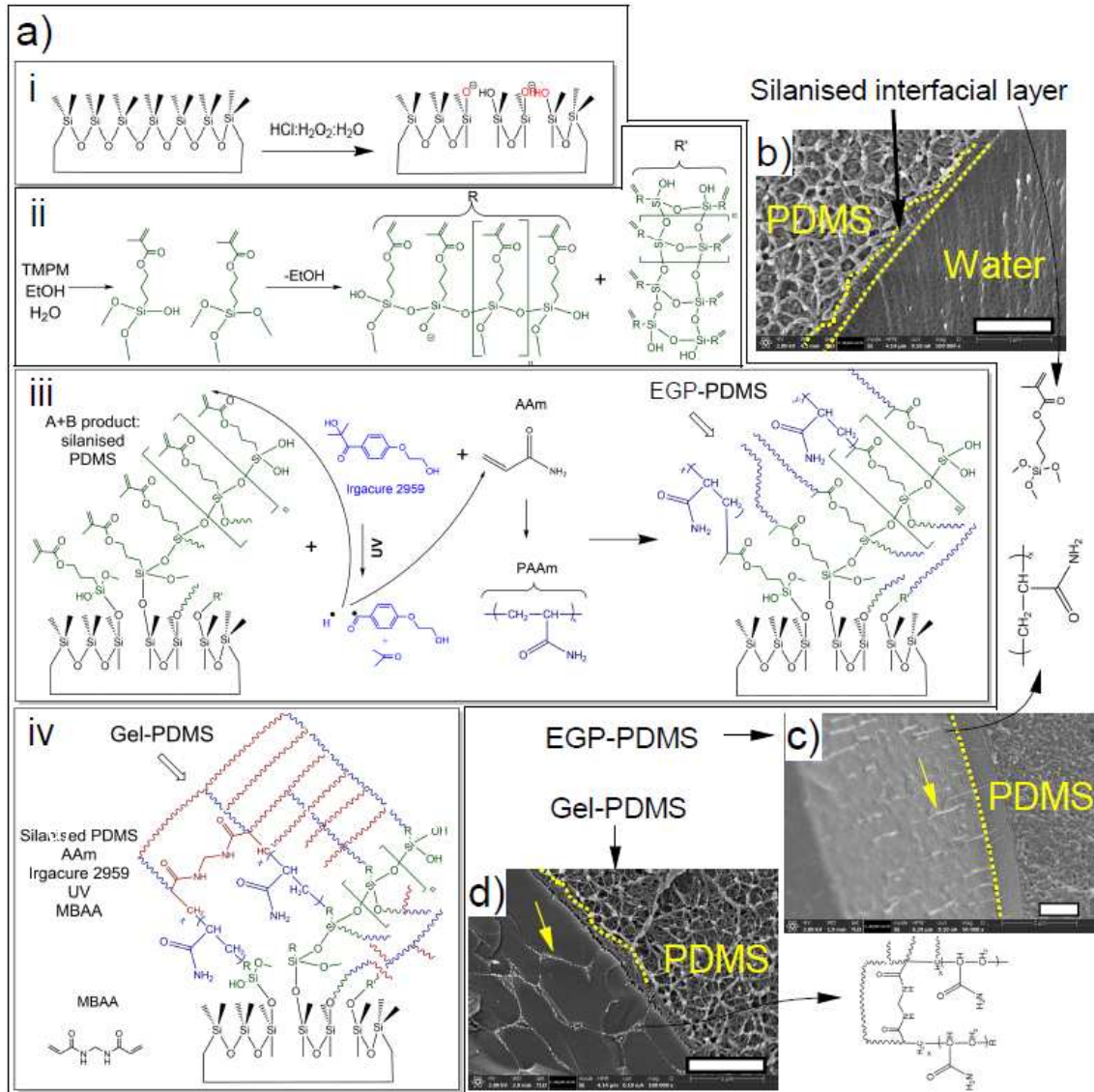
Figure 2. a) Synthesis of EGP/PAAm hydrogel-PDMS elastomer composite and cryo-SEM images from b) silanised, c) end-grafted PAAm and d) hydrogel-grafted porous PDMS elastomers. The images were collected from mid-through cross-section of samples. The scale bar shown in white bars represents 1 μm. The cross-sections above the dashed yellow line present the PDMS elastomeric part of the composite/sponge. The distinguished area between two dashed lines in the panel (b) shows the silanised interfacial layer. The white fibular structure in the panel (c) and the white branched network in the panel (d), pointed with yellow arrows, show grafted AAm polymer chains) and crosslinked AAm polymer chains respectively.

Figure 2(c) presents a cryo-SEM image from EGP-PDMS sponge showing stretched polymer chains of un-crosslinked AAm (pointed with a yellow arrow). This implies a brush configuration (when hydrated), bearing in mind that the cryo process constrains movement/change of the conformation as a result of external stimuli. However, the conformation of EGP may not be confirmed explicitly by cryo-SEM. The crosslinked network of the AAm gel within the gel-PDMS composite is visible in Figure 2(d) which is pointed with a yellow arrow. The porous PDMS resembles the collagen matrix of cartilage and PAAm hydrogel was grafted to impart functionality of proteoglycans in cartilage (i.e. retaining water within the structure) on the composite. More discussion on structural similarities between cartilage and the gel-PDMS composite can be found in SI (Figure S 10).
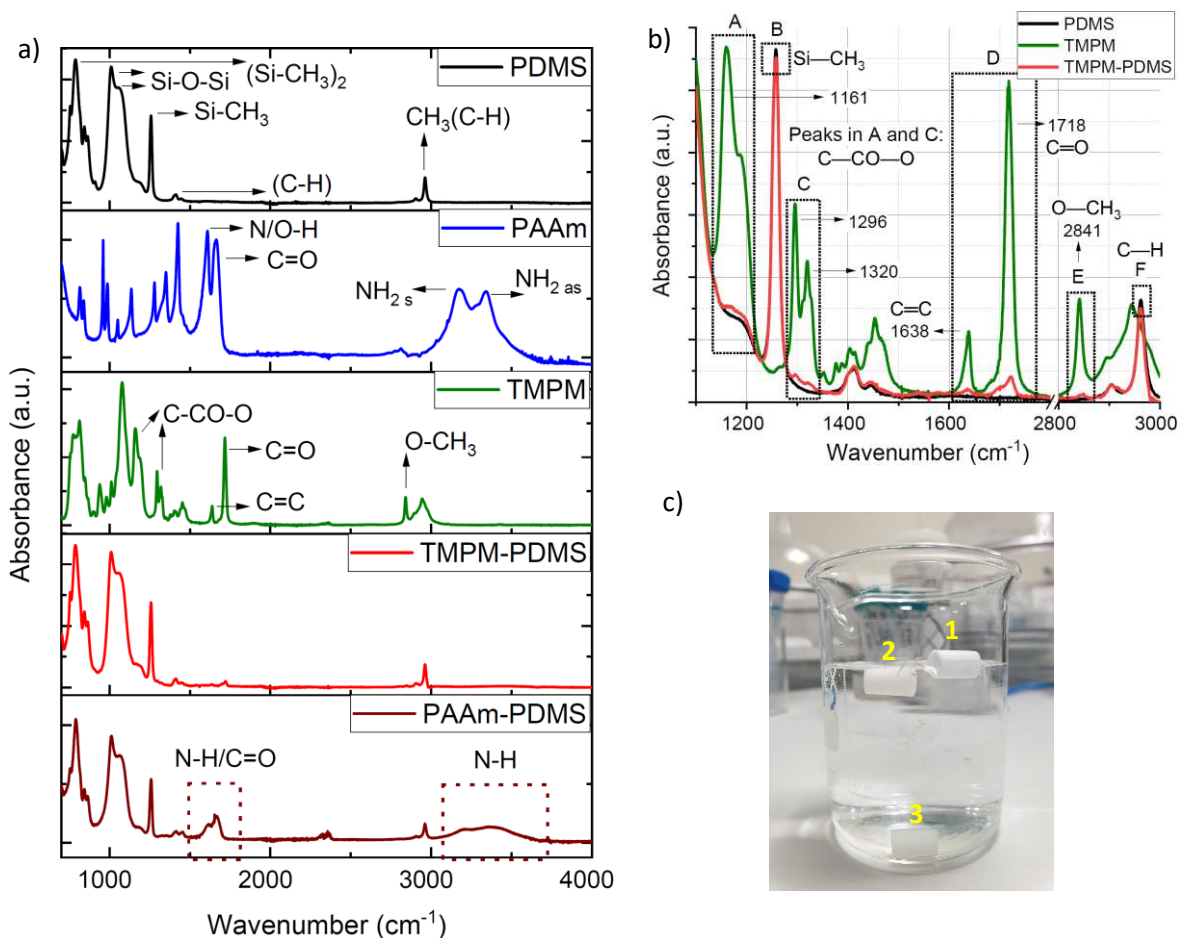
Figure 3. a) ATR-FTIR spectra from PDMS sponge, gel-PDMS composite TMPM treated PDMS sponge and reference materials, b) comparison of ATR-FTIR spectra collected for PDMS and TMPM-PDMS and c) an image showing water exposure of PDMS sponge (1), TMPM-PDMS (2) and gel/EGP-PDMS (3)

ATR-FTIR spectra were obtained for the dehydrated PDMS sponge, the reference PAAm hydrogel, the TMPM-silanised PDMS sponge and the PAAm grafted PDMS sponge materials as shown in Figure 3(a). Distinctive chemical bonds observed for each material are annotated in the spectra. Peak positions associated with the bonds are listed in Table 1. The presence of PAAm in the PAAm-grafted PDMS sponge was confirmed by strong absorptions at 1617 cm^{-1} corresponding to the NH$_2$ bending vibration, 1665 cm^{-1} corresponding to C=O stretching of the —CO—NH$_2$ group and at 3357 and 3203 cm^{-1} characteristics of N—H peaks[51]. Peak positions associated with PDMS sponge remained relatively unchanged (apart from Si—O—Si for PAAm-PDMS) following TMPM and PAAm treatments implying negligible impact of the etching and UV irradiation processes on chemical bonding of the PDMS. This agrees with the cryo-image in Figure 2(b) which shows etching/silane-induced interfacial modification of the PDMS surface less than 100nm thick. This is considerably smaller than the typical depth of analysis of ATR-FTIR (i.e. a few microns). With reference to the PAAm associated peaks, peak positions attributed to the N—H bonds (3342 and 3175 cm^{-1} for reference PAAm) shifted to higher wavelengths in the PAAm-grafted PDMS sponge. The observed shift can originate from residual water in the dehydrated structure due to the increased concentration of hydrogen bonds within the structure[51] or can be an indication of the interactions between PAAm and PDMS.

Table 1. Chemical bond and peak position detected on ATR-FTIR spectra from different sponges and reference materials

Bonding	PDMS	PAAm	TMPM	TMPM-PDMS	PAAm-PDMS
			Peak position (cm^{-1})		
Si—CH$_3$	789, 1258	-	-	789, 1258	790, 1258
Si—O—Si	1011, 1053	-	-	1011, 1053	1013, 1058
C—H	2962, 2905, 1412, 1397	-	-	2962, 2905, 1412	2961, 2907, 1414
N/O—H	-	1610	-	-	1617
N—H	-	3342, 3175	-	-	3357, 3203
C=O	-	1664	-	-	1665
C—CO—O	-	-	1161, 1296, 1320	1162, 1296, 1320	-
C=O	-	-	1718	1721	-
O—CH$_3$	-	-	2841	2847	-
C=C	-	-	1638	1637	-

Figure 3(b) shows the spectra for TMPM and PDMS on their own and their composite with peaks arising from chemical bonds in TMPM marked in regions A, C, D and E. There was a shift to the higher wavelengths for O—CH$_3$ peak in the TMPM-treated PDMS sponge as compared to TMPM reference peaks. This shift can be attributed to hydrolysis of the O—CH$_3$ groups in the Eth:TMPM:H$_2$O solution and subsequent grafting of TMPM to the etched PDMS surface. Regions B and F in Figure 3(b) evidenced a decrease in intensity of Si—CH$_3$ (at 1258) and C—H (at 2962) peaks for the TMPM-treated PDMS sponge when compared the PDMS sponge. The decreased intensity suggests the formation of interfacial silanol groups as a result of the etching process.

Contact angle measurements

Water absorption behaviour of cartilage is an essential factor for its load-bearing and lubrication characteristics[1, 4]. The PDMS elastomer was selected as the matrix because it can restrain water-swelling of the infused hydrogel. Table S 1 in the SI evidences a negligible dimensional change of the gel-PDMS following water-immersion tests over a span of two weeks. The swelling effect has been often observed in hybrid hydrogels which leads to loss of mechanical properties. The PDMS sponge as a bi-phasic structure cannot absorb water due to its hydrophobic nature (Figure 3(c)), lacking a crucial property of cartilage. For composite materials, EGP/gel imparted water absorption to the bi-phasic structure thus mimicking cartilage (Figure 3(c)). In order to investigate water absorption properties of materials, wettability measurements (shown in Figure 4) were carried out using a camera integrated tensiometer. Water contact angle (WCA) for the PDMS sponge exhibited almost super-hydrophobic behaviour with a significantly higher WCA compared to a dense PDMS (Figure S 8(c) in the SI). Super-hydrophobic characteristics can be achieved by tailoring the specific chemistry or texture on surfaces[52]. WCA for the PDMS sponge decreased from 148° to 144° over a period of 20 minutes at atmospheric pressure and room temperature. This implied a transition from Cassie–Baxter (i.e. air exists between the surface grooves and water droplet) to Wenzel states as the trapped air pockets were released and water penetrated into the superficial pores[53-54]. The PAAm chain/gel grafting had a substantial impact on the WCA and resulted in a decrease of the WCA to 22° as the droplet met the material. The WCA decreased over time and the droplet eventually disappeared in less than 2 and 18 minutes for the EGP-PDMS and gel-PDMS respectively. This observation cannot simply be explained by wetting state transition or spreading of water droplets and together with the water droplet volume results (Figure 4) indicates water uptake by the EGP/gel-PDMS materials.
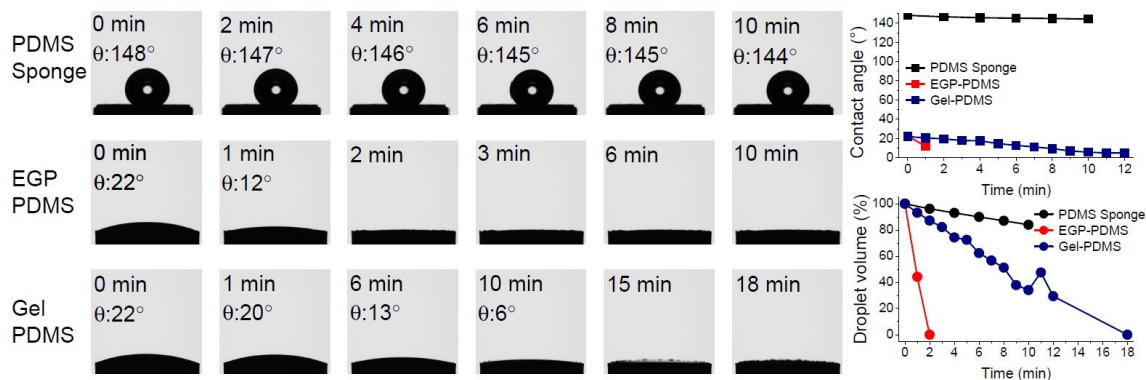
Figure 4. Water contact angle measurements and water intake investigation. Values are presented as the mean of five readings on four samples (n=4×5). The standard deviation for measurements were <7°, <4° and <3° for the PDMS-sponge, EGP-PDMS and gel-PDMS respectively.

Permeation of structures

A permeation cell (Figure 5) was designed and developed in this study for conducting permeability measurements (see materials and methods section and Figure S 3 in the SI). Show in Figure 5, compared to the pristine PDMS sponge, PAAm chain and hydrogel grafting into the sponges reduced water permeability of the structures by one and three orders of magnitude respectively. The permeability of a poroelastic structure determines its stress-relaxation time scales during which the fluid phase contributes to the load bearing capacity[55-57]. The lower permeability of EGP/gel PDMS triggers resistance against fluid flow through the structure and hence is expected to defer the poroelasticity-driven stress-relaxation. This is shown in the next section (Figure 6(a)). For materials with relatively high permeability coefficients (>10^{-12} m^2) fluid exudation occurs in fractions of a second[55-56] and hence ultra-high compression rates are required to capture the fluid pressurisation within the structure.
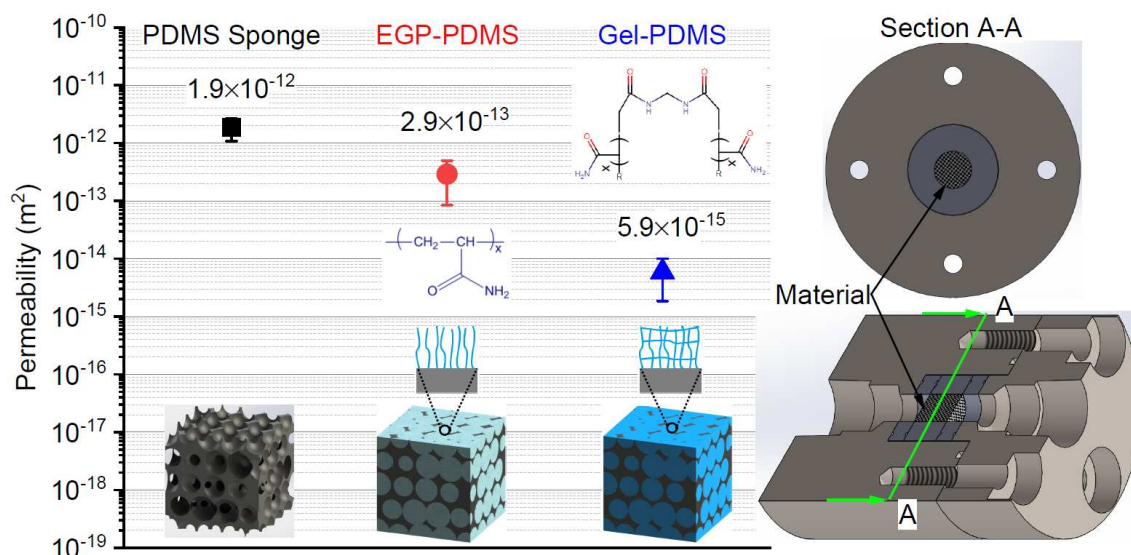
Figure 5. Permeation cell and results for PDMS sponge (1.9±0.8×10^{-12}), brush-PDMS (2.9±2.1×10^{-13}) and gel-PDMS (5.9±4.1×10^{-15}) materials. Values are presented as the mean ± SDs of three measurements on triplicate samples (n=3×3).

In hydrogels, the polymer mesh size controls the permeability[58] which in turn is dominated by crosslinking density and synthesis parameters (i.e. chemistry of the hydrogel)[59]. The EGP-PDMS lacks

chemical crosslinking and, instead exploited interactions between flowing water molecules and extended polymer chains (Figure 2(c)) to reduce the permeability when compared to the PDMS sponge. The gel-PDMS encompassed crosslinked polymer chains (Figure 2(d)). The crosslinked chains generated a polymer network that effectively counteracted water flow bringing about a smaller permeability as compared to the PDMS sponge and EGP-PDMS.

Load bearing properties of the materials

A set-up comprising a flat porous indenter, a flat porous drainage plate, a cylindrical water bath and two mechanical testing equipment were used for compression testing of materials at relatively low (10^{-3} s^{-1} or 16×10^{-3} s^{-1}) and high (1 s^{-1} or 0.83 s^{-1}) strain rates. The experimental setup and loading rates were based on those for cartilage[2, 35-36, 39, 60]. In stress-relaxation experiments, following a tare loading step of 0.2 or 0.5 N, the materials were compressed at a certain rate to 10%-50% strains and maintained at the constant strain for 12 hours until an equilibrium stress state (full relaxation of stresses at each strain) was reached before strain was relaxed. The stress-relaxation time constants were derived through fitting load-time response for materials using (extended)-exponential decay functions[45]. The responses for the material loads over ramp and pause (iso-strain) phases are shown in Figure 6(a) on a logarithmic time scale. The wet-PDMS and dry-PDMS represents conditions where the PDMS sponge was compresses with pores filled with water and air, respectively.

Shown in Figure 6(a), the peak load (i.e. where the maximum load at the maximum strain was recorded; load-bearing behaviour) for the gel-PDMS composite at 1 s^{-1} was greater by a factor of 14 and 3 when compared to the PAAm gel and PDMS sponge, respectively. At the relatively lower strain rate (i.e. 10^{-3} s^{-1}), the load-bearing behaviour was 19 and 3 times greater than the PAAm gel and PDMS sponge, respectively. The EGP-PDMS exhibited a less pronounced impact and a peak load by 50%-80% larger than the PDMS sponge. A freestanding PAAm chain (un-crosslinked) structure dissolves in water and hence measurements were not possible.

When grafted to the PDMS sponge, the EGP-PDMS appeared to possess an 8 to 9-fold greater load-bearing behaviour when compared to the PAAm gel as shown in Figure 6(a). While the load-time curves for the wet-PDMS and dry-PDMS conditions (Figure 6(a)) at 10^{-3} s^{-1} were identical, at 1 s^{-1} a greater peak load was recorded for the wet-PDMS condition. This indicated water pressurisation within the PDMS sponge structure which resisted compression by applying a reactionary force to the load-cell. The stress relaxed poroelastically following a fluid exudation and plateaued at the same stress for the dry-PDMS condition. A relatively high permeability of the PDMS sponge brought about exudation of the fluid during the load-ramp phase and hence impeded the fluid pressurisation at 10^{-3} s^{-1} [55-56]. This led to a negligible stress-relaxation for the PDMS sponge at 10^{-3} s^{-1} as fluid could exit the material without load induced pressurisation owing to the high permeability. In other words, the time required to achieve the maximum strain at 10^{-3} s^{-1} was far larger than the time-frame fluid exudes the structure for the PDMS sponge. Therefore, the load transient response for the PDMS-wet and PDMS-dry conditions were indistinguishable at 10^{-3} s^{-1}.

The stress-relaxation characteristics of the materials showed that the PAAm gel and gel-PDMS experienced two incidents of stress-relaxation at similar time scales (τ_1 and τ_2). Shown in Figure 6(a), it transpired that the first relaxation occurred within the one second of the pause phase at both strain rates. The second relaxation appeared at around 3000 s and 3670-3770 s for the gel-PDMS and PAAm gel respectively. These can be attributed to the time dependant processes associated with viscoelastic and poroelastic relaxation processes[45]. No significant change in the stress-relaxation time constants was observed as a function of strain rate for those studied here. Cartilage[2] and enhanced hydrogels[43] have been shown to undergo two distinct stress-relaxation processes similar to what can be observed

in iso-strain part of the Figure *6*(a). The characteristic relaxation time scales (τ) of 0.77 and 162 s were derived for glenohumeral cartilage through a biphasic quasi-linear viscoelastic model developed by Huang et al.[2]. Although the τ_1 for cartilage is close to that of the gel-PDMS (0.82-0.88), τ_2 for the gel-PDMS was over one order of magnitude greater than of that for cartilage. The obtained τ_2 value for the gel-PDMS is a valid observation in the scope of hydrogels. Prolonged stress-relaxation time scales on the order of 1000 s and above have been shown in chemically crosslinked hydrogels[45, 61]. For example, Chan et al. observed poroelastic relaxation times in order of 1000 s for a polyethylene glycolmethacrylate hydrogel[45]. Alongside the chemistry (e.g. crosslinking density) of a hydrogel which influences stress-relaxation time scales, the testing configuration (e.g. compression depth) has been shown to impact the time scale[61]. Kalcioglu et al.[61] reported that it could take more than 6 hr for a complete stress-relaxation of a PAAm hydrogel following a 400 um indentation. Therefore, a greater indention depth in this study (3000 μm) as compared to a 50-μm indention depth in the cartilage study by Huang et al. could be a contributing factor to the large τ_2 observed for the gel-PDMS.

An enormous amount of research has succeeded in enhancing mechanical properties of hydrogels towards achieving moduli greater than that of cartilage and skin[7, 34, 62], with a minor focus on the stress-relaxation behaviour of the improved hydrogels[43]. A hallmark of cartilage is its stress-relaxation behaviour. This prevents mechanical damage to cartilage[43] and engender exceptional load-bearing properties[2] and lubricity[1]. The extent of stress-relaxation from the peak stress within a loading cycle correlates to the fluid pressurisation within the structure and hence is an indicative of its load-bearing behaviour and energy dissipation[2, 55-56]. Huang et al.[2] performed relatively fast ramp (strain rate of around 1 s^{-1}) compression tests on bovine cartilage from glenohumeral joints to a strain limit of 5% following a tare load of 0.89 N. They observed a peak stress of 0.92-0.95 MPa which later fully damped the stress and relaxed to almost its initial tare load within a 1000 s hold phase. The peak stress at a considerably lower strain rate (i.e. 0.125x10^{-3} s^{-1}) was an order of magnitude smaller as compared to the higher strain rate compression and the stress was relaxed by 70%. These demonstrate the crucial role of stress-relaxation behaviour of cartilage on its load-bearing properties and underpin the observations showing that up to 90% of the stress in cartilage is carried through fluid pressurisation[2]. In a study[43] where stress-relaxation of a DN hydrogel was investigated, the gel relaxed only 10%-30% of the applied load following a quick loading (400 ms ramp phase) during the hold phase. This implies that the modulus of a modified hydrogel can be of the same order as cartilage, but it might lack the load-bearing features of cartilage. In our study, compared to the study by Sun et al.[43], we observed a significantly greater stress-relaxation of around 55% from the peak stress at the strain rate of 1 s^{-1}, however, it is evident that more work is required in this aspect to achieve load-bearing properties in close proximity to that of cartilage.

Compressive modulus of the materials

While peak loads for materials enhanced by increasing the strain rate, equilibrium loads (the measured load following the complete stress-relaxation at a certain strain) appeared to be almost independent of the strain rate (Figure *6*(a)). This indicates that the peak modulus can vary depending on the applied strain rate, while an equilibrium modulus can be independent of the strain rate for the test conditions defined in this study. The elastic compressive modulus was determined from the linear derivative of the stress–strain curves at 0.1-0.3 and 0.3-0.5 strain ranges for peak stress and equilibrium stress states at a strain rate of 0.83 s^{-1} (Figure *6*(b)). A greater modulus was observed at the higher strain range (i.e. strain stiffening) which has also been reported for toughened hydrogels[3] and cartilage[60]. Cartilage exhibits a strain stiffening behaviour which is crucial for its load-bearing performance[43]. The strain stiffening of the gel-PDMS can be attributed to the fluid pressurisation within the gel upon compression[43] and viscoelastic response of the PDMS sponge. The gel-PDMS was

substantially stiffer than the PAAm-gel (the peak modulus was around 19 and 48 kPa at 0.1-0.3 and 0.3-0.5 strain ranges) and exhibited a peak modulus of 0.91 and 2.54 MPa at 0.1-0.3 and 0.3-0.5 strain ranges respectively. The gel-PDMS composite was above 3-4 times stiffer than the PDMS sponge over both strain ranges. At the equilibrium state, the gel-PDMS composite was approximately 2 and 50 times stiffer than the PDMS-sponge and PAAm gel materials over both strain ranges respectively. The equilibrium modulus for the gel-PDMS at 0.1-0.3 was 452 kPa which was within the range of equilibrium modulus reported in the literature for cartilage under unconfined compression conditions [35-37, 39, 60].

Mechanical parameters of cartilage are influenced by its properties (e.g. water content[39]) and the testing procedure (i.e. confined, unconfined or indentation[2, 36, 39], testing direction due to anisotropy[35] and the strain limit[60]). A few studies reported a Young modulus between 0.2 and 0.8 MPa for cartilage in normal direction to its articulating surfaces[35-37]. Korhonena et al.[36] performed unconfined compression steps of 5% strain each up to a total strain of 20% at a strain rate of around 0.7×10^{-3} s^{-1} on bovine's humeral, patellar and femoral cartilage plugs. They reported Young's moduli of 0.3-0.8 MPa for the cartilage plugs. The peak and equilibrium stresses at 5% were around 50 and 10 kPa respectively. Julkunen et al. [39] conducted a similar unconfined compression testing on human articular knee patellar cartilage plugs at a strain rate of approximately 0.28×10^{-3}-0.45×10^{-3} s^{-1} to a total strain limit of 15% inclusive of a 5% pre-strain step. At a total strain limit of 10% a peak stress of 80-120 kPa was shown which is close to a peak stress of around 52-55 kPa observed for the gel-PDMS material at a strain rate and limit of 10^{-3} s^{-1} and 10% respectively. Jurvelin et al.[35] extracted cartilage discs from human patello-femoral joint and compressed the cartilage discs in a series of 16-step stress-relaxation cycles to a strain limit of 20% at 10^{-3} s^{-1} in an unconfined configuration. The equilibrium Young's modulus (10%-20% strain range) was shown to be around 581 kPa which is comparable to the equilibrium modulus of 452 kPa observed for the gel-PDMS material. The equilibrium stresses at 10% and 20% strain were around 20 and 80 kPa which are close to the equilibrium stresses of 44 and 89 kPa obtained for the gel-PDMS in this study. These, therefore, confirm that the equilibrium modulus of the gel-PDMS (452 kPa at a strain limit of 30%) is within the range of values reported for cartilage.

In another study by Loy et al.[60], five consecutive confined compression steps of 10% strain each with a tare load of 0.1N were performed on human glenoid and humeral head cartilage plugs at a compression rate of 0.25 μm/s (i.e. 0.1×10^{-3}-0.2×10^{-3} s^{-1}). Compressive aggregate moduli at 0 and 16% strain (confined moduli) of 229-370 and 0.351-0.543 kPa were reported for the plugs which are in the same order of the compressive modulus observed for the gel-PDMS material (Figure *6*(b)). A more detailed comparison between compressive modulus of the gel-PDMS composite and the moduli reported for bovine, swine and human cartilage can be found in Table S 2 in the SI. The peak stress at the third strain step (30% strain) was around 170 kPa which relaxed to just below 120 kPa over a 600 s pause phase (~30% relaxation from the peak stress). The aggregate modulus (confined compression) for a cartilage material has shown to be in the same order of the Young's modulus of cartilage (unconfined compression) with the former being slightly greater than the later[35-37]. For the gel-PDMS material a peak and equilibrium stress of 215 and 125 kPa was observed at 30% strain and a strain rate of 10^{-3} (40% relaxation from the peak stress). The observed peak and equilibrium stresses and the extent of stress-relaxation from the peak load for the gel-PDMS material at a relatively low compression rate (i.e. 10^{-3} s^{-1}) is therefore, in the same order of that reported for cartilage.
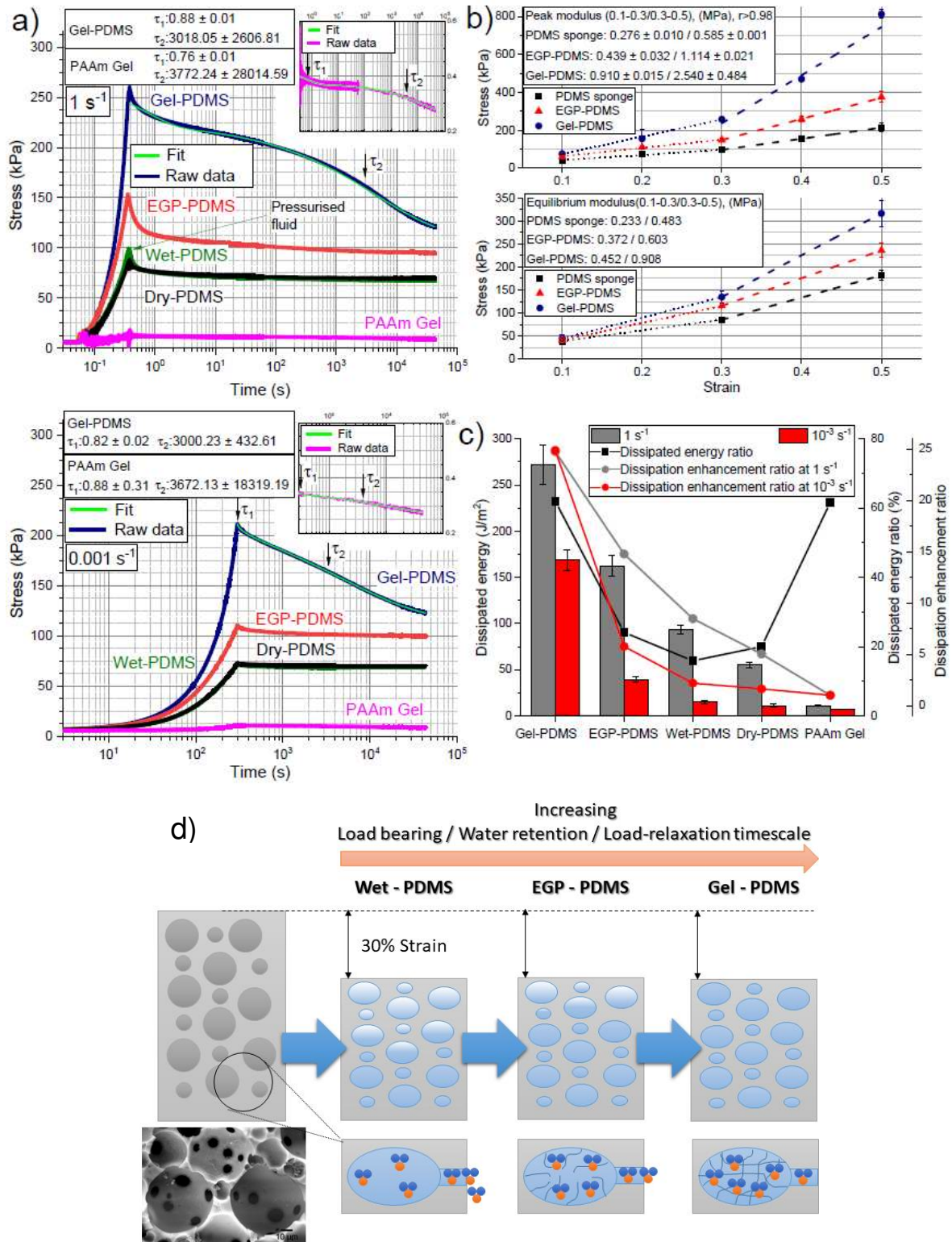
Figure *6*. a) Load-time graphs for compression and stand-still stress-relaxation at 30% strain for PAAm gel, PDMS sponge and EGP/gel-PDMS composites. b) Elastic moduli (linear derivative of the stress–strain curve) of materials within two strain ranges of 0.1-0.3 and 0.3-0.5 at a strain rate of 0.83 s^{-1} (nominal stress σ= $F/\pi r^2$). At each strain the maximum stress and the stress after complete stress-relaxation processes were used to obtain the peak and equilibrium modulus respectively. c) Energy dissipation results given by the hysteresis loop with loading to a strain limit of 30% and unloading after the load-response was fully relaxed (full-capacity energy dissipation) at two strain rates of 1 and 10^{-3} s^{-1}. Dissipation energy ratio presents the ratio of the energy dissipation at 10^{-3} s^-

^{1} to 1 s^{-1} for each individual material. Dissipation energy enhancement ratio presents the energy dissipation for materials normalised to the energy dissipation in PAAm gel within a loading-unloading cycle. Tests were carried out at fully swollen state and materials were immersed in water bath during tests (except the dry-PDMS tests). The values present mean and SD of the measurements (n=3×3). d) presents a schematic of load-bearing/toughening mechanisms for the materials. Compression drives fluid exudation in the wet-PDMS and water molecules (orange/blue triple circles) are compelled to leave the pores. Grafted PAAm chains in EGP/Gel-PDMS materials prompt resistance to fluid flow by osmotic interactions.

Capacity of the materials to dissipate energy

As can be seen in Figure 6(b), the equilibrium modulus for the PDMS sponge was 43 and 102 kPa smaller than its peaks modulus at the strain range of 0.1-0.3 and 0.30-.5 (corresponding to 15%-17% reduction), respectively. This reduction in modulus was above an order of magnitude larger for the gel-PDMS composite (458 and 1632 kPa corresponding to 50%-65% reduction). Accordingly, it can be inferred that the stress-relaxation and resultant energy dissipation capacity of the PDMS sponge was enhanced by PAAm grafting. The energy dissipation characteristics for the materials were evaluated at a strain limit of 30% (Figure 6(c)). At 1 s^{-1}, the capacity of the gel-PDMS composite to dissipate the applied energy appeared to be approximately 25, 5 and 3 times greater as compared to that of PAAm-gel, dry-PDMS and wet-PDMS materials/conditions respectively. At 10^{-3} s^{-1}, these ratios rose to a higher level compared to the PDMS sponge and were 25, 15 and 11 times greater in each case. This denotes the beneficial influence of gel grafting at relatively slow compression loadings. The greater capacity to dissipate energy in the gel-PDMS composite can be attributed to its lower permeability leading to extended poroelasticity-driven stress-relaxation.

Dissipation energy values for the PDMS sponge, compared to the PAAm gel, are presented in Figure 6(c) (dissipation enhancement ratio) showing that the dissipated energy was 5.0-8.5 times and 1.6-2.2 times higher at the 1 s^{-1} and 10^{-3} s^{-1} respectively. At 1 s^{-1}, water pressurisation during the compression of the PDMS sponge when the pores were filled with water (i.e. the wet-PDMS condition) contributed to 40% of the total energy dissipation occurred for wet-PDMS condition. Similar to the PDMS sponge, for the EGP-PDMS a larger enhancement to the energy dissipation was observed at the higher strain rate (1 s^{-1}). The dissipation enchantment ratio for the EGP-PDMS was around 15 and 6 at 1 s^{-1} and 10^{-3} s^{-1} respectively. This is rooted in a relatively higher permeability of the PDMS sponge and EGP-PDMS compared to the gel-PDMS which resulted in an increased contribution of pressurised fluid to the total load at higher compression rates[55-57]. The AAm polymer chain grafting into the PDMS sponge enhanced energy dissipation with a more pronounced influence at the relatively low strain rate of 10^{-3} s^{-1}. Through AAm polymer chain grafting, the dissipated energy (with respect to the wet-PDMS condition) increased by 164% and 74% at 10^{-3} s^{-1} and 1 s^{-1} respectively. This observation can be partly ascribed to the lower permeability of the EGP-PDMS material which brought about fluid pressurisation within the brush-PDMS structure even at 10^{-3} s^{-1} where the fluid pressurisation for the PDMS sponge was negligible[55, 57]. The fluid pressurisation escalated energy dissipation through fluid exudation[55].

The dissipated energy ratio in Figure 6(c) was defined as the ratio of the energy dissipation at 10^{-3} s^{-1} to that at 1 s^{-1}. The higher ratio suggests efficiencies at relatively slow compressions and larger poroelastic stress-relaxation time constants. As shown in Figure 6(c), the dissipated energy ratio for the gel-PDMS and PAAm-gel was almost identical (62%). This denotes that the contribution of the prolonged stress-relaxation constituent (poroelastic relaxation) to the total stress-relaxation was the same for both materials. Consequently, it can be deduced that the poroelasticity (long-term stress-relaxation) was bestowed upon the gel-PDMS by the infused gel. This agrees with the observed results (Figure 5 and Figure 6(a)) showing lower permeability of the gel-PDMS as compared to the EGP-PDMS

and PDMS sponge and similar stress-relaxation time constants for the gel-PDMS and PAAm-gel materials. These results enable us to present a load-bearing/toughening mechanism for materials (the schematic illustration shown in Figure 6(d)). The manufactured PDMS-sponge offers 'intrinsic' permeability and resistance to fluid flow and compression drives fluid exudation. The EGP-PDMS retains water within its pores by un-crosslinked PAAm polymer. The osmotic interactions produce relatively greater resistance to fluid flow when compared to PDMS sponge. Crosslinked PAAm hydrogel further decreases permeability and water migration through the porosity. This brings about prolonged load-relaxation properties and greater load-bearing behaviour when compared to EGP-PDMS.

Cyclic compression testing behaviour of the materials

The recovery of load-bearing behaviour of the gel-PDMS and PDMS sponge was rigorously examined through ten continuous compression cycles. The cyclic compression tests were carried out at two strain rates of 0.83 s^{-1} and 16x10^{-3} s^{-1} which are presented in Figure 7(a and b) respectively. The dissipated energy and load-recovery within each cycle are summarised with the figure insets.

Greater hysteresis characteristics were observed for the gel-PDMS as compared to the PDMS sponge. The nonlinear load-strain curve observed in the gel-PMDS data has been evidenced for cartilage[63] implying strain-stiffening behaviour. All the cyclic graphs were almost identical for the PDMS sponge at both strain rates. For the PDMS sponge, the peak-load recovery between cycle 2 and 10 was discerned to remain beyond 97% and 99% at 0.83 s^{-1} and 16x10^{-3} s^{-1} respectively. A slight reduction in the dissipated energy (17-30%) compared to the first cycle was observed for cycles 2 to 10. For gel-PDMS, compressed at 0.83 s^{-1}, at the second cycle a 4.2% and 24% reduction in the peak-load and energy dissipation was observed respectively. A notable difference either in the energy dissipation or the peak-load recovery was not found for cycles between 2 and 10. The peak-load recovery stayed above 95% and energy dissipation remained above 74% for these cycles. Additional experiments (shown in Figure S 4 in the SI), in which unloading phases returned to an absolute zero position (zero tare load) and consecutive cycles started from there, showed superimposed curves with the load-recovery staying above 98% and a slight reduction to the dissipated energy (≤4% at 0.83 s^{-1}). At 16x10^{-3} s^{-1}, the decay of load-bearing properties of the gel-PDMS material was negligible. The peak-load recovery for cycles between 2 and 10 was higher than 98% and a maximum reduction of 14% was observed in the energy dissipation. In order to obtain insights into the cyclic loading behaviour of the composite at longer timescales, the gel-PDMS and PDMS-sponge materials were further investigated up to 100 compression cycles (with no pause phase). This can be found in Figure S 11 in SI showing promising cyclic loading (compression) properties of the gel-PDMS under conditions defined in this study. The PAAm gel material was deformed following the first cycle of compression and hence immediate cyclic loading was not feasible.

The attested superb load-recovery properties of the gel-PDMS composite can be attributed to the elastic properties of the stiffer component of the composite; i.e. PDMS sponge. The elastic behaviour of PDMS sponge hinders its plastic deformation during repeatable uniaxial compressions[49]. Therefore, the gel-PDMS recovered to its initial shape and size immediately after the load was released prompting an eminent recovery of the load-bearing behaviour. The grafted hydrogel within the gel-PDMS structure had to catch up with the elastic defamation/recovery of the PDMS sponge during loading/unloading. Therefore, the PDMS matrix of the gel-PDMS accelerates fluid exudation during loading and facilitates regaining the exuded fluid (reswelling) during unloading. These were manifested in Figure 6(a) (i.e. a smaller τ_2 value for the gel-PDMS as compared to that for the PAAm gel) and Figure 7 (i.e. the immediate recovery). Furthermore, the PDMS matrix of the gel-PDMS composite mitigated the prominent drawback of hydrogel systems; that is the swelling effect. The

modified hydrogels often suffer loss of mechanical properties once immersed in water due to the osmotic pressure-driven swelling[25]. This loss can range from trivial to considerable extent. The PDMS matrix is a resilient structure when exposed to most aqueous reagents[64] especially water. The non-swelling nature of PDMS in aqueous environments restrained the hydrogel expansion in water. Therefore, the gel-PDMS maintained its shape and size in aqueous mediums regardless of immersion time hindering swelling-induced loss of mechanical properties.
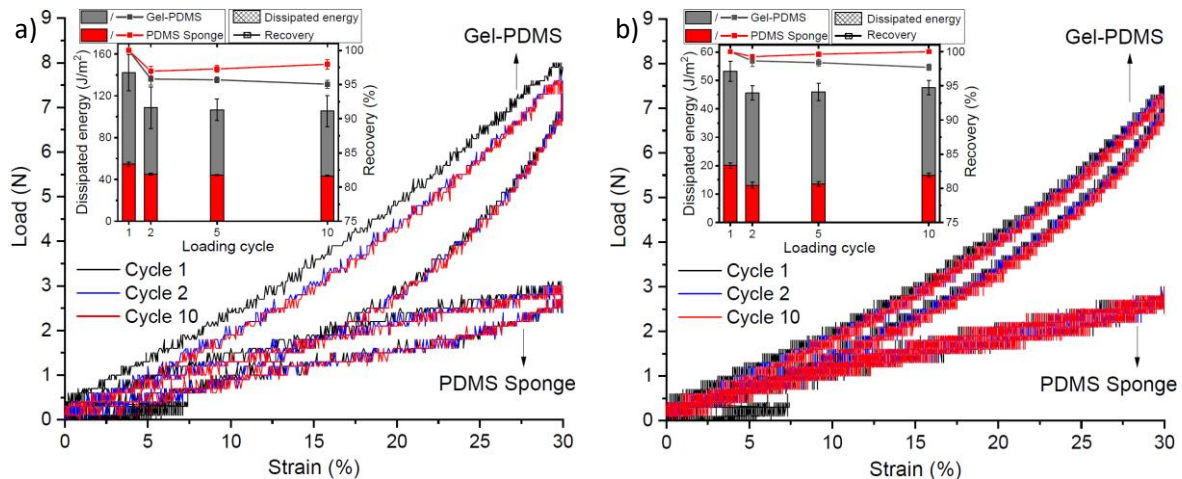
Figure 7. Load-strain curves for cyclic compression testing of the gel-PDMS and PDMS sponge (dry-PDMS condition) materials to a strain limit of 30% with a 15-second pause phase included in between the loading and unloading phases at strain rates of a) 0.83 s⁻¹ and b) 16x10⁻³ s⁻¹. Graphs for cycles 1, 2 and 10 are only presented for clarity since there was no noticeable difference between cycles 2 to 10. The 2ⁿᵈ to 10ᵗʰ cycles consecutively started from the tare load immediately following an unloading phase to tare load with no waiting time. The inset in the graph shows the dissipated energy during each cycle (column) and the peak-load recovery (ratio of the peak-load at each cycle to the peak-load at the first cycle which is presented by symbol-line). The column bars and line graphs in insets present mean and SD of the measurements (n=3×3).

Finally, the current approach taken in this study tackles some of the concerns involved with hydrogels (i.e. swelling and load/shape-recovery) and it provides opportunities for improvements towards a structure with more similarities to native cartilage. Cartilage possesses anisotropic behaviour[35] (e.g. the directional orientation of fibrils is different in surface from that in bulk[39]) with more water content at the surface and stiffer structure deeper towards the subchondral bone[39]. These make biomimicry of cartilage more arduous. Highly ordered hydrogels can impart anisotropic behaviour to engineered structures[17]. For example, anisotropic functionality has been achieved through incorporation of cofacially oriented metal-oxide nanosheets[65] or physically crosslinking stretched hydrogels containing semirigid polyelectrolytes[66]. The PDMS sponge can function as a scaffold to graft-infuse anisotropic hydrogels to advance the composite towards structures with properties akin to cartilage.

Conclusion

A novel approach was taken in this study to mimic the structure and properties of cartilage. A porous PDMS was used to restrain the expansion and deformation of an infused-grafted hydrogel (i.e. PAAm). The gel-PDMS composite was resilient to water-swelling and cyclic compression loading. Therefore, loss of mechanical properties as a result of osmotic swelling was mitigated and ultra-fast recovery behaviour was bestowed on the composite. Cyclic compression testing showed that the load-bearing and energy-dissipation capacity recovered to 95-98% and 74-96% of their initial values respectively, immediately with no waiting time between cycles.

By leveraging prolonged stress-relaxation characteristics of PAAm and the elastic behaviour of the crosslinked PDMS, the capacity of energy dissipation of the composite was improved by approximately 25 times that of the PAAm hydrogel system and 3-11 times that of the PDMS sponge system. The composite showed two distinct stress-relaxation processes with EGP-PDMS showing a better proximity to cartilage in terms of poroelastic stress-relaxation time constants. The PAAm gel grafting decreased permeability of the PDMS sponge by three orders of magnitude, thereby fluid pressurisation within a prolonged time-frame was enabled. The load bearing capacity at 30% strain was, as a result, enhanced by 14-19 and 3 folds when compared to the PAAm gel and PDMS sponge materials. The composite exhibited an elastic modulus of 452 kPa which is within the range of the modulus values reported for cartilage. The composite has the capacity to undergo stress-relaxation to an extent of 40-55% from the maximum stress at 30% strain. This, in some cases, surpassed the extent of stress-relaxation in some of previously developed hydrogels and is comparable to that of cartilage (30-95%).

The PAAm grafting tuned the structure to absorb water in the steady-state condition which brought about the capability to regain the exuded fluid as found in cartilage. An intermediate structure between the composite and the PDMS sponge was fabricated based-on grafting un-crosslinked PAAm polymer chains (i.e. EGP-PDMS). The EGP-PDMS possessed inferior mechanical properties as compared to the gel-PDMS, while showing faster water absorption behaviour and stress-relaxation characteristics. We believe this study is a paradigmatic of a structure that can function as a hydrogel while can retain its properties, shape and geometry in harsh load-bearing applications. Therefore, this study triggers development of advanced materials built on stiff hydrophobic-soft hydrophilic framework for applications operating in aqueous environments.

Supporting Information: includes further details and data pertaining to size distribution of PMMA particles, UV/Vis analysis of the dense PDMS and PDMS sponge, the setup for permeability measurement, cyclic compression tests, ATR-FTIR and X-ray elemental mapping analysis to confirm the complete dissolution of the PMMA template, fabrication method, swelling tests and a comparison table comparing the wide range of mechanical properties for cartilage reported in literature.

References
(1) Moore, A. C.; Burris, D. L. Tribological Rehydration of Cartilage and Its Potential Role in Preserving Joint Health. *Osteoarthritis Cartilage* **2017,** *25* (1), 99-107.
(2) Huang, C.-Y.; Soltz, M. A.; Kopacz, M.; Mow, V. C.; Ateshian, G. A. Experimental Verification of the Roles of Intrinsic Matrix Viscoelasticity and Tension-Compression Nonlinearity in the Biphasic Response of Cartilage. *J. Biomech. Eng.* **2003,** *125* (1), 84-93.
(3) Calvert, P. J. A. m. Hydrogels for Soft Machines. *Adv. Mater.* **2009,** *21* (7), 743-756.
(4) Chen, M.; Briscoe, W. H.; Armes, S. P.; Klein, J. J. s. Lubrication at Physiological Pressures by Polyzwitterionic Brushes. *Science* **2009,** *323* (5922), 1698-1701.
(5) Lanigan, J.; Fatima, S.; Charpentier, T.; Neville, A.; Dowson, D.; Bryant, M. J. B. Lubricious Ionic Polymer Brush Functionalised Silicone Elastomer Surfaces. *Biotribology* **2018,** *16,* 1-9.

(6) Li, A.; Benetti, E. M.; Tranchida, D.; Clasohm, J. N.; Schönherr, H.; Spencer, N. D. J. M. Surface-Grafted, Covalently Cross-Linked Hydrogel Brushes with Tunable Interfacial and Bulk Properties. *Macromolecules* **2011,** *44* (13), 5344-5351.

(7) Lin, P.; Zhang, R.; Wang, X.; Cai, M.; Yang, J.; Yu, B.; Zhou, F. Articular Cartilage Inspired Bilayer Tough Hydrogel Prepared by Interfacial Modulated Polymerization Showing Excellent Combination of High Load-Bearing and Low Friction Performance. *ACS Macro Lett.* **2016,** *5* (11), 1191-1195.

(8) Ma, S.; Scaraggi, M.; Wang, D.; Wang, X.; Liang, Y.; Liu, W.; Dini, D.; Zhou, F. Nanoporous Substrate-Infiltrated Hydrogels: A Bioinspired Regenerable Surface for High Load Bearing and Tunable Friction. *Adv. Funct. Mater.* **2015,** *25* (47), 7366-7374.

(9) Gombert, Y.; Simič, R.; Roncoroni, F.; Dübner, M.; Geue, T.; Spencer, N. D. Structuring Hydrogel Surfaces for Tribology. *Adv. Mater. Interfaces* **2019,** *6* (22), 1901320.

(10) Zhang, P.; Zhao, C.; Zhao, T.; Liu, M.; Jiang, L. Recent Advances in Bioinspired Gel Surfaces with Superwettability and Special Adhesion. *Advanced Science* **2019,** *6* (18), 1900996.

(11) Moutos, F. T.; Freed, L. E.; Guilak, F. A Biomimetic Three-Dimensional Woven Composite Scaffold for Functional Tissue Engineering of Cartilage. *Nat. Mater* **2007,** *6* (2), 162-167, DOI: 10.1038/nmat1822.

(12) Ng, K. W.; Ateshian, G. A.; Hung, C. T. Zonal Chondrocytes Seeded in a Layered Agarose Hydrogel Create Engineered Cartilage with Depth-Dependent Cellular and Mechanical Inhomogeneity. *Tissue Eng. Part A* **2009,** *15* (9), 2315-2324.

(13) Liao, I. C.; Moutos, F. T.; Estes, B. T.; Zhao, X.; Guilak, F. Composite Three-Dimensional Woven Scaffolds with Interpenetrating Network Hydrogels to Create Functional Synthetic Articular Cartilage. *Adv. Funct. Mater.* **2013,** *23* (47), 5833-5839.

(14) Zhao, W.; Jin, X.; Cong, Y.; Liu, Y.; Fu, J. Degradable Natural Polymer Hydrogels for Articular Cartilage Tissue Engineering. *J. Chem. Technol. Biotechnol.* **2013,** *88* (3), 327-339.

(15) Arakaki, K.; Kitamura, N.; Fujiki, H.; Kurokawa, T.; Iwamoto, M.; Ueno, M.; Kanaya, F.; Osada, Y.; Gong, J. P.; Yasuda, K. Artificial Cartilage Made from a Novel Double-Network Hydrogel: In Vivo Effects on the Normal Cartilage and Ex Vivo Evaluation of the Friction Property. *J Biomed Mater Res A* **2010,** *93* (3), 1160-1168.

(16) Zhang, Y. S.; Khademhosseini, A. Advances in Engineering Hydrogels. *Science* **2017,** *356* (6337), eaaf3627, DOI: 10.1126/science.aaf3627 %J Science.

(17) Zhao, Z.; Fang, R.; Rong, Q.; Liu, M. Bioinspired Nanocomposite Hydrogels with Highly Ordered Structures. *Adv. Mater.* **2017,** *29* (45), 1703045.

(18) Wang, J.; Lin, L.; Cheng, Q.; Jiang, L. A Strong Bio-Inspired Layered Pnipam–Clay Nanocomposite Hydrogel. *Angew. Chem.* **2012,** *51* (19), 4676-4680.

(19) Okumura, Y.; Ito, K. The Polyrotaxane Gel: A Topological Gel by Figure-of-Eight Cross-Links. *Adv. Mater.* **2001,** *13* (7), 485-487.

(20) Haraguchi, K.; Takehisa, T. Nanocomposite Hydrogels: A Unique Organic–Inorganic Network Structure with Extraordinary Mechanical, Optical, and Swelling/De-Swelling Properties. *Adv. Mater.* **2002,** *14* (16), 1120-1124.

(21) Gong, J. P.; Katsuyama, Y.; Kurokawa, T.; Osada, Y. Double-Network Hydrogels with Extremely High Mechanical Strength. *Adv. Mater.* **2003,** *15* (14), 1155-1158.

(22) Huang, T.; Xu, H.; Jiao, K.; Zhu, L.; Brown, H. R.; Wang, H. A Novel Hydrogel with High Mechanical Strength: A Macromolecular Microsphere Composite Hydrogel. *Adv. Mater.* **2007,** *19* (12), 1622-1626.

(23) Sakai, T.; Matsunaga, T.; Yamamoto, Y.; Ito, C.; Yoshida, R.; Suzuki, S.; Sasaki, N.; Shibayama, M.; Chung, U.-i. Design and Fabrication of a High-Strength Hydrogel with Ideally Homogeneous Network Structure from Tetrahedron-Like Macromonomers. *Macromolecules* **2008,** *41* (14), 5379-5384.

(24) Sun, T. L.; Kurokawa, T.; Kuroda, S.; Ihsan, A. B.; Akasaki, T.; Sato, K.; Haque, M. A.; Nakajima, T.; Gong, J. P. Physical Hydrogels Composed of Polyampholytes Demonstrate High Toughness and Viscoelasticity. *Nat. Mater* **2013,** *12* (10), 932-937, DOI: 10.1038/nmat3713.

(25) Yang, Y.; Wang, X.; Yang, F.; Wang, L.; Wu, D. Highly Elastic and Ultratough Hybrid Ionic–Covalent Hydrogels with Tunable Structures and Mechanics. *Adv. Mater.* **2018,** *30* (18), 1707071.

(26) Sun, J.-Y.; Zhao, X.; Illeperuma, W. R.; Chaudhuri, O.; Oh, K. H.; Mooney, D. J.; Vlassak, J. J.; Suo, Z. Highly Stretchable and Tough Hydrogels. *Nature* **2012,** *489* (7414), 133.

(27) Li, J.; Illeperuma, W. R.; Suo, Z.; Vlassak, J. J. Hybrid Hydrogels with Extremely High Stiffness and Toughness. *ACS Macro Lett.* **2014,** *3* (6), 520-523.

(28) Yu, H. C.; Li, C. Y.; Du, M.; Song, Y.; Wu, Z. L.; Zheng, Q. Improved Toughness and Stability of K-Carrageenan/Polyacrylamide Double-Network Hydrogels by Dual Cross-Linking of the First Network. *Macromolecules* **2019,** *52* (2), 629-638.

(29) Lin, P.; Zhang, T.; Wang, X.; Yu, B.; Zhou, F. Freezing Molecular Orientation under Stretch for High Mechanical Strength but Anisotropic Hydrogels. *Small* **2016,** *12* (32), 4386-4392.

(30) Lin, P.; Ma, S.; Wang, X.; Zhou, F. Molecularly Engineered Dual-Crosslinked Hydrogel with Ultrahigh Mechanical Strength, Toughness, and Good Self-Recovery. *Adv. Mater.* **2015,** *27* (12), 2054-2059.

(31) Yang, C. H.; Wang, M. X.; Haider, H.; Yang, J. H.; Sun, J.-Y.; Chen, Y. M.; Zhou, J.; Suo, Z. Strengthening Alginate/Polyacrylamide Hydrogels Using Various Multivalent Cations. *ACS Appl. Mater. Interfaces* **2013,** *5* (21), 10418-10422.

(32) Hu, X.; Vatankhah-Varnoosfaderani, M.; Zhou, J.; Li, Q.; Sheiko, S. S. Weak Hydrogen Bonding Enables Hard, Strong, Tough, and Elastic Hydrogels. *Adv. Mater.* **2015,** *27* (43), 6899-6905.

(33) Wang, Y. J.; Zhang, X. N.; Song, Y.; Zhao, Y.; Chen, L.; Su, F.; Li, L.; Wu, Z. L.; Zheng, Q. Ultrastiff and Tough Supramolecular Hydrogels with a Dense and Robust Hydrogen Bond Network. *Chem. Mater.* **2019,** *31* (4), 1430-1440.

(34) Rauner, N.; Meuris, M.; Zoric, M.; Tiller, J. C. Enzymatic Mineralization Generates Ultrastiff and Tough Hydrogels with Tunable Mechanics. *Nature* **2017,** *543* (7645), 407-410.

(35) Jurvelin, J.; Buschmann, M.; Hunziker, E. Mechanical Anisotropy of the Human Knee Articular Cartilage in Compression. *Proc. Inst. Mech. Eng. Pt. H J. Eng. Med.* **2003,** *217* (3), 215-219.

(36) Korhonen, R.; Laasanen, M.; Töyräs, J.; Rieppo, J.; Hirvonen, J.; Helminen, H.; Jurvelin, J. Comparison of the Equilibrium Response of Articular Cartilage in Unconfined Compression, Confined Compression and Indentation. *J. Biomech.* **2002,** *35* (7), 903-909.

(37) Machado, J.; Viriato, N.; Marta, M.; Vaz, M. Experimental Characterization of the Mechanical Properties of Knee Articular Cartilages in Compression: First Approach with Swine Tissues. *Rheumatology and Orthopedic Medicine* **2017,** *2* (4), 1-4.

(38) Xu, X.; Jerca, F. A.; Jerca, V. V.; Hoogenboom, R. Covalent Poly(2-Isopropenyl-2-Oxazoline) Hydrogels with Ultrahigh Mechanical Strength and Toughness through Secondary Terpyridine Metal-Coordination Crosslinks. *Adv. Funct. Mater.* **2019,** *29* (48), 1904886, DOI: 10.1002/adfm.201904886.

(39) Julkunen, P.; Wilson, W.; Jurvelin, J. S.; Rieppo, J.; Qu, C.-J.; Lammi, M. J.; Korhonen, R. K. Stress–Relaxation of Human Patellar Articular Cartilage in Unconfined Compression: Prediction of Mechanical Response by Tissue Composition and Structure. *J. Biomech.* **2008,** *41* (9), 1978-1986.

(40) Cutcliffe, H. C.; DeFrate, L. E. Comparison of Cartilage Mechanical Properties Measured During Creep and Recovery. *Sci. Rep.* **2020,** *10* (1), 1-8.

(41) Zhang, H.; Bian, C.; Jackson, J. K.; Khademolhosseini, F.; Burt, H. M.; Chiao, M. Fabrication of Robust Hydrogel Coatings on Polydimethylsiloxane Substrates Using Micropillar Anchor Structures with Chemical Surface Modification. *ACS Appl. Mater. Interfaces* **2014,** *6* (12), 9126-9133.

(42) Visser, J.; Melchels, F. P.; Jeon, J. E.; Van Bussel, E. M.; Kimpton, L. S.; Byrne, H. M.; Dhert, W. J.; Dalton, P. D.; Hutmacher, D. W.; Malda, J. Reinforcement of Hydrogels Using Three-Dimensionally Printed Microfibres. *Nature communications* **2015,** *6* (1), 1-10.

(43) Sun, W.; Xue, B.; Li, Y.; Qin, M.; Wu, J.; Lu, K.; Wu, J.; Cao, Y.; Jiang, Q.; Wang, W. Polymer-Supramolecular Polymer Double-Network Hydrogel. *Adv. Funct. Mater.* **2016,** *26* (48), 9044-9052.

(44) Wu, L.; Zhuang, Z.; Li, S.; Ma, X.; Diao, W.; Bu, X.; Fang, Y. Ultrastretchable, Super Tough, and Rapidly Recoverable Nanocomposite Double-Network Hydrogels by Dual Physically Hydrogen Bond

and Vinyl-Functionalized Silica Nanoparticles Macro-Crosslinking. *Macromol. Mater. Eng.* **2019,** *304* (5), 1800737, DOI: 10.1002/mame.201800737.

(45) Chan, E. P.; Deeyaa, B.; Johnson, P. M.; Stafford, C. M. Poroelastic Relaxation of Polymer-Loaded Hydrogels. *Soft Matter* **2012,** *8* (31), 8234-8240.

(46) Wu, D.; Xu, F.; Sun, B.; Fu, R.; He, H.; Matyjaszewski, K. Design and Preparation of Porous Polymers. *Chem. Rev.* **2012,** *112* (7), 3959-4015.

(47) He, H.; Averick, S.; Mandal, P.; Ding, H.; Li, S.; Gelb, J.; Kotwal, N.; Merkle, A.; Litster, S.; Matyjaszewski, K. Multifunctional Hydrogels with Reversible 3d Ordered Macroporous Structures. *Advanced Science* **2015,** *2* (5), 1500069.

(48) Xia, Y.; Gates, B.; Yin, Y.; Lu, Y. Monodispersed Colloidal Spheres: Old Materials with New Applications. *Adv. Mater.* **2000,** *12* (10), 693-713.

(49) Lee, K. Y.; Chun, J.; Lee, J.-H.; Kim, K. N.; Kang, N.-R.; Kim, J.-Y.; Kim, M. H.; Shin, K.-S.; Gupta, M. K.; Baik, J. M.; Kim, S.-W. Hydrophobic Sponge Structure-Based Triboelectric Nanogenerator. *Adv. Mater.* **2014,** *26* (29), 5037-5042, DOI: 10.1002/adma.201401184.

(50) Yang, J.; Bai, R.; Chen, B.; Suo, Z. Hydrogel Adhesion: A Supramolecular Synergy of Chemistry, Topology, and Mechanics. *Adv. Funct. Mater.* **2020,** *30* (2), 1901693, DOI: 10.1002/adfm.201901693.

(51) Liu, R.; Liang, S.; Tang, X.-Z.; Yan, D.; Li, X.; Yu, Z.-Z. Tough and Highly Stretchable Graphene Oxide/Polyacrylamide Nanocomposite Hydrogels. *J. Mater. Chem.* **2012,** *22* (28), 14160-14167.

(52) Kreder, M. J.; Alvarenga, J.; Kim, P.; Aizenberg, J. Design of Anti-Icing Surfaces: Smooth, Textured or Slippery? *Nature Reviews Materials* **2016,** *1* (1), 1-15.

(53) Mishra, H.; Schrader, A. M.; Lee, D. W.; Gallo Jr, A.; Chen, S.-Y.; Kaufman, Y.; Das, S.; Israelachvili, J. N. Time-Dependent Wetting Behavior of Pdms Surfaces with Bioinspired, Hierarchical Structures. *ACS Appl. Mater. Interfaces* **2016,** *8* (12), 8168-8174.

(54) Murakami, D.; Jinnai, H.; Takahara, A. Wetting Transition from the Cassie–Baxter State to the Wenzel State on Textured Polymer Surfaces. *Langmuir* **2014,** *30* (8), 2061-2067.

(55) de Boer, G. N.; Raske, N.; Soltanahmadi, S.; Dowson, D.; Bryant, M. G.; Hewson, R. W. A Porohyperelastic Lubrication Model for Articular Cartilage in the Natural Synovial Joint. *Tribol. Int.* **2020,** *149*, 105760, DOI: https://doi.org/10.1016/j.triboint.2019.04.044.

(56) de Boer, G.; Hewson, R.; Bryant, M.; Dowson, D. An Investigation into the Contact between Soft Elastic and Poroelastic Bodies Rotating under Load. *Tribology - Materials, Surfaces & Interfaces* **2017,** *11* (4), 193-201.

(57) de Boer, G. N.; Raske, N.; Soltanahmadi, S.; Bryant, M. G.; Hewson, R. W. Compliant-Poroelastic Lubrication in Cartilage-on-Cartilage Line Contacts. *Tribology - Materials, Surfaces & Interfaces* **2020**, 1-15, DOI: 10.1080/17515831.2020.1720381.

(58) Dunn, A. C.; Sawyer, W. G.; Angelini, T. E. Gemini Interfaces in Aqueous Lubrication with Hydrogels. *Tribology Letters* **2014,** *54* (1), 59-66.

(59) Brannon-Peppas, L.; Harland, R. S. *Absorbent Polymer Technology*, Elsevier: 2012.

(60) Loy, B. N.; Zimel, M.; Gowda, A. L.; Tooley, T. R.; Maerz, T.; Bicos, J.; Guettler, J. A Biomechanical and Structural Comparison of Articular Cartilage and Subchondral Bone of the Glenoid and Humeral Head. **2018,** *6* (7), 2325967118785854.

(61) Kalcioglu, Z. I.; Mahmoodian, R.; Hu, Y.; Suo, Z.; Van Vliet, K. From Macro-to Microscale Poroelastic Characterization of Polymeric Hydrogels Via Indentation. *Soft Matter* **2012,** *8* (12), 3393-3398.

(62) Zhang, D.; Yang, F.; He, J.; Xu, L.; Wang, T.; Feng, Z.-Q.; Chang, Y.; Gong, X.; Zhang, G.; Zheng, J. Multiple Physical Bonds to Realize Highly Tough and Self-Adhesive Double-Network Hydrogels. *ACS Appl. Polym. Mater.* **2020,** *2* (3), 1031-1042, DOI: 10.1021/acsapm.9b00889.

(63) Mow, V. C.; Kuei, S.; Lai, W. M.; Armstrong, C. G. Biphasic Creep and Stress Relaxation of Articular Cartilage in Compression: Theory and Experiments. *J. Biomech. Eng.* **1980,** *102* (1), 73-84.

(64) Zhu, D.; Handschuh-Wang, S.; Zhou, X. Recent Progress in Fabrication and Application of Polydimethylsiloxane Sponges. *J. Mater. Chem. A* **2017,** *5* (32), 16467-16497, DOI: 10.1039/C7TA04577H.

(65) Liu, M.; Ishida, Y.; Ebina, Y.; Sasaki, T.; Hikima, T.; Takata, M.; Aida, T. An Anisotropic Hydrogel with Electrostatic Repulsion between Cofacially Aligned Nanosheets. *Nature* **2015,** *517* (7532), 68-72.

(66) King, D. R.; Takahashi, R.; Ikai, T.; Fukao, K.; Kurokawa, T.; Gong, J. P. Anisotropic Double-Network Hydrogels Via Controlled Orientation of a Physical Sacrificial Network. *ACS Appl. Polym. Mater.* **2020,** *2* (6), 2350-2358, DOI: 10.1021/acsapm.0c00290.